Watt-level europium laser at 703 nm

Pavel Loiko, Daniel Rytz, Sebastian Schwung, Patrick Pues, Thomas Jüstel, Jean-Louis Doualan, Patrice Camy

Watt-level Europium laser at 703 nm

Pavel Loiko,[1] Daniel Rytz,[2] Sebastian Schwung,[2] Patrick Pues,[3] Thomas Jüstel,[3] Jean-Louis Doualan,[1] and Patrice Camy[1,*]

[1]*Centre de Recherche sur les Ions, les Matériaux et la Photonique (CIMAP), UMR 6252 CEA-CNRS-ENSICAEN, Université de Caen Normandie, 6 Boulevard du Maréchal Juin, 14050 Caen Cedex 4, France*
[2]*EOT GmbH, Struthstraße 2, D-55743, Idar-Oberstein, Germany*
[3]*Department of Chemical Engineering, Münster University of Applied Sciences, Stegerwaldstraße 39, D-48565 Steinfurt, Germany*
**Corresponding author: patrice.camy@ensicaen.fr*

Received XX Month XXXX; revised XX Month, XXXX; accepted XX Month XXXX; posted XX Month XXXX (Doc. ID XXXXX); published XX Month XXXX

We report on a watt-level highly efficient Europium laser operating at the $^5D_0 \rightarrow {}^7F_4$ transition. It is based on the stoichiometric $KEu(WO_4)_2$ crystal. Under pumping by a green laser at 532.1 nm, the $KEu(WO_4)_2$ laser generated a maximum peak output power of 1.11 W at ~703 nm with a slope efficiency of 43.2% and a linear polarization ($E \parallel N_m$). A laser threshold as low as 64 mW was achieved. True continuous-wave operation was demonstrated. The polarized emission properties of monoclinic $KEu(WO_4)_2$ were determined. 2021 Optical Society of America

http://dx.doi.org/10.1364/OL.99.099999

During the past years, there is a great interest for the development of visible solid-state lasers based on such rare-earth ions as Pr^{3+}, Tb^{3+}, Dy^{3+}, Sm^{3+} or Eu^{3+} [1].

Trivalent Europium ions (Eu^{3+}, electronic configuration: $[Xe]4f^6$) are featuring multi-color emissions in the visible (orange, red and deep red) due to transitions from the metastable $^5D_0$ state to a group of lower-lying ^7F_J (J = 0...6) energy-levels ($^7F_0$ is the ground-state), Fig. 1. Among them, the $^5D_0 \rightarrow {}^7F_2$ transition at ~612 nm is typically the most intense one which determines the use of Eu^{3+} ions as activators of red phosphors with high color purity [2] for applications in white LEDs [3,4]. The metastable $^5D_0$ state exhibits a relatively long lifetime (in the ms-range) and weak non-radiative relaxation even in high-phonon-energy matrices leading to high luminescence quantum yields [4]. Intense absorption bands of Eu^{3+} ions in the blue and UV allow for their efficient excitation, e.g., by GaN diodes. The Eu^{3+} ions are also known as structural markers [5], as the $^5D_0 \rightarrow {}^7F_2$ transition of purely electric-dipole nature is a hypersensitive one (its intensity depends on the site symmetry and its distortion).

At a glance, Eu^{3+} ions appear attractive for the development of low-threshold red lasers with a quasi-four-level scheme. However, to date, only few studies were dedicated to Eu lasers. The first laser action in Eu^{3+} (at the $^5D_0 \rightarrow {}^7F_2$ transition) was achieved in 1963 by Chang using a $Eu:Y_2O_3$ single-crystal cooled to 77 K to reduce the thermal population of the lower laser level [6]. In 2004, Park *et al.* demonstrated room-temperature (RT) stimulated-emission at 620 nm in Eu^{3+}-doped semiconductor GaN thin-films on sapphire [7,8]. In 2007, Nakamura *et al.* reported on RT lasing from polymer films containing Eu^{3+} complexes [9]. In 2011, Bagayev *et al.* achieved pulsed RT lasing (at the $^5D_0 \rightarrow {}^7F_4$ transition) in a $Eu:KGd(WO_4)_2$ single-crystal [10]. Shortly after that, quasi continuous-wave (CW) and CW operation of this crystal and its isomorph, $Eu:KY(WO_4)_2$, were obtained [11,12].

So far, the best result achieved with a highly-doped (25 at.%) $Eu:KGd(WO_4)_2$ crystal comprised a peak output power of 54 mW at 702.3 nm with a slope efficiency of ~4.6% [11]. The authors developed a frequency-doubled Nd laser at 533.6 nm (pumping into the short-living $^5D_1$ state, Fig. 1) suffering from thermo-optic problems. Recently, lasing in Eu^{3+}-doped $LiYF_4$ was demonstrated leading to still low output of 15 mW at 701.9 nm with a similar slope efficiency [13]. A frequency-doubled 393.5 nm Ti:Sapphire laser (pumping into the higher-lying $^5L_6$ state, Fig. 1) was used, however, such pumping leads to stronger heat loading and may induce color centers in oxide crystals.

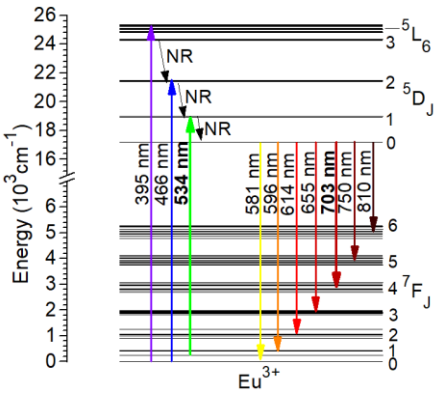

Fig. 1. The scheme of energy-levels of Eu^{3+} ions showing possible pump and laser transitions. NR – non-radiative relaxation. The crystal-field splitting corresponds to $KY(WO_4)_2$.

The main difficulty for power scaling of Eu lasers in [11,13] was the selection of an appropriate pump source. The Eu^{3+} transitions in absorption falling in the visible and UV spectral ranges ($^7FJ \rightarrow {}^5D_{J'}$, $^5L_{J'}$, $^5G_{J'}$) are spin-forbidden and their intensities are weak [14]. The corresponding spectral linewidths are also narrow. Thus, for achieving high pump absorption, one must adjust precisely the pump wavelength (~0.1 nm) or ensure very high Eu^{3+} doping.

In the present work, we aimed at reconsidering Eu^{3+} ions for efficient and power-scalable continuous-wave RT lasers operating in the deep red spectral range. For that, as a gain material, we have used the $KEu(WO_4)_2$ crystal and as a pump source – a commercial high-power 532 nm laser. This compound belongs to the crystal family of monoclinic double tungstates (MDTs) $KRE(WO_4)_2$ which are known as excellent host matrices for doping with rare-earth ions [15]. Their advantages are the following: (i) long RE^{3+} - RE^{3+} interatomic distances leading to weak luminescence quenching; (ii) high doping concentrations up to stoichiometric (100 at.%) compositions; (iii) strong polarization anisotropy of absorption and stimulated-emission spectra [14] and (iv) suitable thermo-optical properties for certain crystal cuts [16] (nearly athermal behavior). These properties are particularly interesting for the stoichiometric $KEu(WO_4)_2$ crystal.

The single crystal of $KEu(WO_4)_2$ was grown by the Top-Seeded Solution Growth method [17] using potassium ditungstate ($K_2W_2O_7$) as a solvent. The starting reagents were K_2CO_3, WO_3 and Eu_2O_3 (4N purity) taken according to the solute : solvent mass ratio of 1:5. The growth started at 1228 K. A [010] seed crystal was used. The as-grown crystal, Fig. 2(a), was pink colored due to Eu^{3+} ions. $KEu(WO_4)_2$ is monoclinic (sp. gr. C^6_{2h} – $C2/c$, No. 15), its lattice constants are a = 1069.88(7) Å, b = 046.87(5) Å, c = 760.47(5) Å and β = 130.774(4)°. Eu^{3+} ions are residing in a single type of sites with the C_2 symmetry and VIII-fold oxygen coordination. According a single-crystal X-ray diffraction study, there are no vacancies in the Eu^{3+} site. No signs of Eu^{2+} species were observed as well. Thus, the Eu^{3+} ion density was calculated to be $N_{Eu} = 61.55\times10^{20}$ cm^{-3} using the measured density of 7.07 g/cm^3.

Monoclinic $KEu(WO_4)_2$ is optically biaxial. Its optical properties are described in the optical indicatrix frame {N_p, N_m, N_g}. The N_p axis is parallel to the ***b***-axis (C_2 symmetry axis) and the other two axes are lying in the ***a***-***c*** plane, Fig. 2(b). The angle N_g ^ ***c*** = 18.5°, measured outside of the monoclinic angle β.

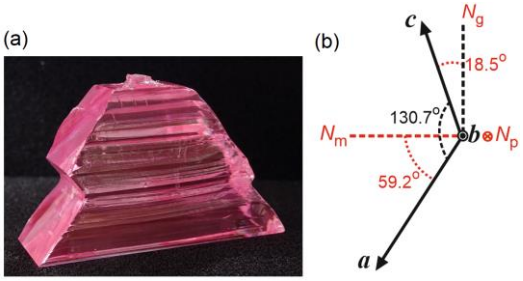

Fig. 2. (a) Photograph of the as-grown $KEu(WO_4)_2$ crystal (length: 40 mm, weight: 61 g, growth direction: along [010]); (b) the scheme of its optical orientation: N_p, N_m, N_g – optical indicatrix axes, ***a***, ***b***, ***c*** – crystallographic axes.

First, we studied polarized spectroscopic properties of Eu^{3+} ions in $K(Y_{1-x}Eu_x)(WO_4)_2$ crystals. The absorption cross-section, σ_{abs}, spectra for the $^7F_{0,1} \rightarrow {}^5D_1$ transitions in the green are shown in Fig. 3(a). For Eu^{3+} ions, due to the small energy separation between the lower-lying multiplets $^7F_{1,2}$ and the ground-state $^7F_0$, the former ones are thermally populated at RT. For transitions from the $^7F_1$ state, the maximum σ_{abs} is 1.71×10^{-20} cm^2 at 534.2 nm and the corresponding absorption bandwidth (full width at half maximum, FWHM) is only 0.6 nm (for ***E*** || N_m). The measurements were done for a $KY_{0.8}Eu_{0.2}(WO_4)_2$ crystal to avoid saturation of the detector.

The stimulated-emission (SE) cross-section, σ_{SE}, spectra for the $^5D_0 \rightarrow {}^7F_2$ and $^5D_0 \rightarrow {}^7F_4$ transitions are shown in Fig. 3(b). They were calculated using the Füchtbauer–Ladenburg (F-L) equation assuming a radiative lifetime of the $^5D_0$ state τ_{rad} = 0.49 ms [17] and the luminescence branching ratios $B(JJ')$ = 83.7% (0 → 2) and 12.8% (0 → 4) [14]. For the latter transition, the maximum σ_{SE} is 1.11×10^{-20} cm^2 at 702.4 nm and the emission bandwidth (FWHM) is ~1 nm (for ***E*** || N_m). The σ_{SE} spectra exhibit a significant anisotropy which is a prerequisite for linearly polarized laser emission.

The RT luminescence decay curve from the $^5D_0$ state of Eu^{3+} ions in $KEu(WO_4)_2$ is single-exponential with a lifetime τ_{lum} of 0.479 ms, see Fig. 3(c). Almost no reduction of the lifetime is observed as compared to the crystal containing 20 at.% Eu. The lifetime of the $^5D_1$ pump level was estimated from the luminescence risetime to be ~4 μs.

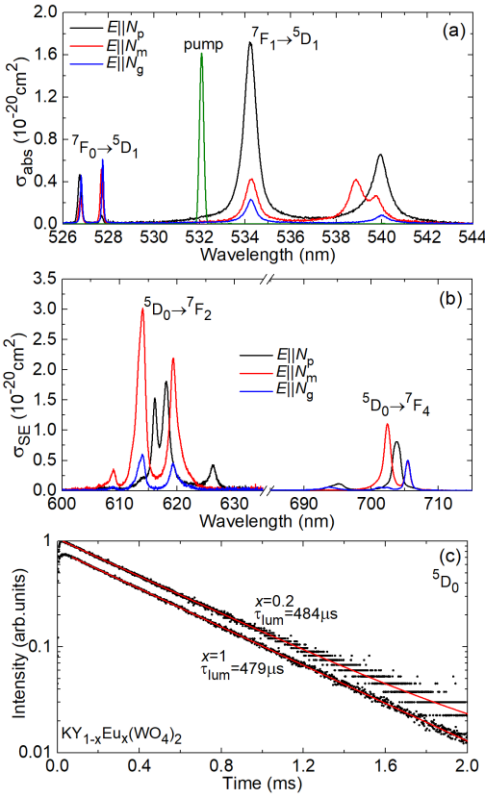

Fig. 3. Spectroscopy of Eu^{3+} ions in monoclinic $K(Y_{1-x}Eu_x)(WO_4)_2$ crystals: (a) polarized absorption cross-sections, σ_{abs}, for the $^7F_{0,1} \rightarrow {}^5D_1$ transition (x = 0.2); (b) polarized stimulated-emission cross-sections, σ_{SE}, for the $^5D_0 \rightarrow {}^7F_{2,4}$ (x = 1); (c) luminescence decay from the $^5D_0$ state (x = 0.2 and 1). In (a), the spectrum of the pump green laser is shown for comparison.

The parallelepipedic laser element from the $KEu(WO_4)_2$ crystal had the dimensions of 4.75(N_p)×5.07(N_m)×5.21(N_g) mm^3. All six faces were polished and remained uncoated. The element was oriented for light propagation along the N_g optical indicatrix axis (N_g-cut). This cut provides access to polarizations $\boldsymbol{E} \parallel N_m$ and $\boldsymbol{E} \parallel N_p$ and ensures nearly athermal behavior (i.e., weak and positive thermal lens). A linear laser cavity was composted of a flat pump mirror (PM) providing a transmission T = 86.0% at 532 nm and high reflection (HR, R >99.5%) at 595-710 nm and a set of output couplers (OCs) having a transmission T_{OC} at 703 nm in the range of 0.3% - 4.3%. Two cavity geometries were used: (i) a hemispherical cavity was terminated by a concave OC (radius of curvature of -50 mm) with the crystal placed near the PM at a ~1 mm airgap; (ii) the plano-plano cavity contained flat PM and OC placed as close as possible to the crystal, Fig. 4. The radii of the laser mode in the crystal were calculated using the ABCD method and they amounted to 55±5 μm and 40±5 μm, respectively.

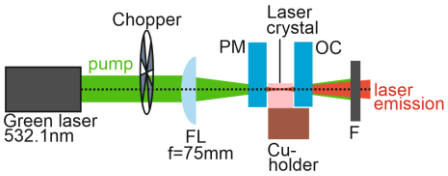

Fig. 4. Scheme of the compact $KEu(WO_4)_2$ laser: L – achromatic focusing lens, PM – pump mirror, OC – output coupler, F -cut-off filter.

The laser crystal was mounted on a passively cooled Cu-holder using silver paste for better heat removal. As a pump source, we used a green laser (Verdi G series, Coherent) emitting up to 9 W of linearly polarized emission at 532.1 nm (linewidth: <0.1 nm) in the fundamental mode ($M^2 \approx 1$). This corresponded to pumping into the $^5D_1$ Eu^{3+} state, Fig. 3(a). The pump was focused into the crystal using an achromatic lens (AC254-X-A series, Thorlabs) coated for high transmission (HT, T > 99.5%) at 532 nm. Lenses with the focal lengths f in the range of 50 - 100 mm were tested. The pump polarization in the crystal corresponded to $\boldsymbol{E} \parallel N_m$. The measured pump absorption, η_{abs} = 59.5±0.5%, was weakly dependent on the pump power. The pumping was in a single pass. The pump was modulated using a chopper (frequency: 25 Hz, duty cycle: 1:4, pump pulse duration: ~10 ms) for quasi-CW operation.

The laser output was filtered from the residual pump using a long-pass filter (FEL600, Thorlabs). The laser emission spectra were measured using an optical spectrum analyzer (OSA, Ando AQ6315-E). The temporal behavior of the laser output was studied using a fast InGaAs photodetector (UPD-5N-IR2-P) and an 8 GHz digital oscilloscope (DSA70804B, Tektronix).

At first, the optimum focusing lens was selected employing a hemispherical cavity and the available OC (T_{OC} = 4.3%). The best performance was achieved for f = 75 mm (pump spot size: $2w_P$ = 75±5 μm, measured by the optical knife method at the 1/e^2 level). The laser generated a maximum peak output power of 0.532 W at 703 nm with a slope efficiency η of 34.1% (vs. the absorbed pump power) and a laser threshold P_{th} of 565 mW, Fig. 5(a). The use of lenses with shorter focal lengths (f = 50 - 60 mm) leading to smaller pump spot sizes resulted in reduced thresholds (412 mW for f = 50 mm) whilst with lower η attributed to poorer mode-matching. Longer f of 100 mm resulted in a rapid increase of the threshold to 722 mW. Thus, the 75 mm lens was selected.

Due to the availability of mirrors, the effect of the output coupling on the laser performance was studied in a plano-plano cavity, Fig. 5(b). The laser operation in such a cavity is possible due to the positive thermal lens expected for N_g-cut $KEu(WO_4)_2$ crystal, similarly to other MDTs. The Eu laser generated a maximum peak output power of 1.11 W at 703 nm with a slope efficiency of 43.2% and a laser threshold of 183 mW (for T_{OC} = 2.4%). At the maximum incident pump power of 4.70 W, the optical-to-optical conversion efficiency η_{opt} amounted to 23.6%. The achieved η value was lower than the Stokes efficiency under lasing conditions, $\eta_{StL} = \lambda_P/\lambda_L$ = 75.7%, indicating a further room for improvement. The input-output dependence was linear up to at least 4.70 W of the incident pump power. Further power scaling was limited to avoid the risk of thermal fracture of the passively cooled crystal. With reducing T_{OC} from 4.3% to 0.3%, the laser threshold gradually decreased from 285 mW to only 64 mW. Such a low laser threshold is due to the quasi-four level laser scheme of the $^5D_0 \rightarrow {}^7F_4$ transition.

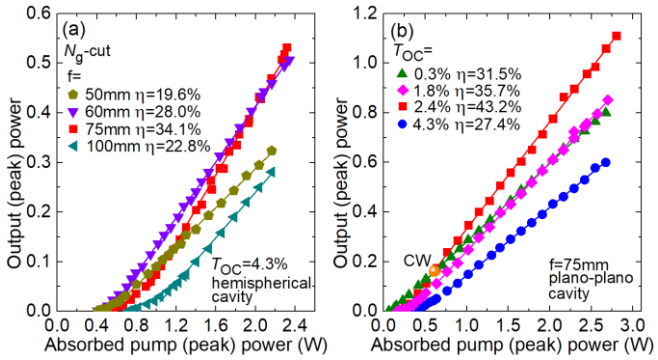

Fig. 5. Input-output dependences for the $KEu(WO_4)_2$ laser operating on the $^5D_0 \rightarrow {}^7F_4$ transition: (a) effect of the focal length of the focusing lens f, hemispherical cavity, T_{OC} = 4.3%; (b) effect of the output coupling T_{OC}, plano-plano cavity, f = 75 mm. N_g-cut crystal. Quasi-CW regime, duty cycle: 1:4. *Orange circle* – true CW operation, T_{OC} = 2.4%.

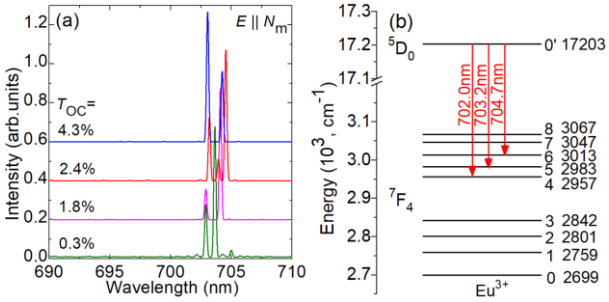

Fig. 6. (a) Typical spectra of laser emission from the $KEu(WO_4)_2$ laser (plano-plano cavity). The laser polarization is $\boldsymbol{E} \parallel N_m$; (b) crystal-field splitting of the $^5D_0$ and $^7F_4$ Eu^{3+} multiplets, *arrow* – the laser transition.

The laser emission was linearly polarized; the polarization state ($\boldsymbol{E} \parallel N_m$) was naturally selected by the anisotropy of the gain, cf. Fig. 3(b). The laser wavelength (~703 nm) was weakly dependent on T_{OC}, see Fig. 6(a). The crystal-field splitting of the $^5D_0$ and $^7F_4$ Eu^{3+} multiplets revealed at low temperature (6 K) is shown in Fig. 6(b). For C_2 sites, each $^{2S+1}L_J$ multiplet with integer J will be split into $2J$+1

sub-levels. The observed laser emission wavelengths are assigned to electronic transitions 0' ($^5D_0$) → 4, 5 and 6 ($^7F_4$). The multi-peak spectral behavior is due to the etalon effects at the crystal / mirror interfaces.

True CW operation was also studied. The incident pump power was limited to ~1 W. Using the smallest T_{OC} = 0.3%, the maximum output power reached 162 mW in good agreement with the quasi-CW regime, Fig. 5(b).

A typical oscilloscope trace of the CW laser is shown in Fig. 7(a). The CW regime was established within ~1 ms after switching on the pump. The slow intensity variations are due to instabilities in the pump green laser.

The typical profile of the laser mode in the far-field (plano-plano cavity) measured at the maximum CW output power is shown in Fig. 7(b). The corresponding 1D intensity profiles were well fitted with the Gaussian distribution. The beam is slightly elliptic, and it is extended along the N_p axis. This is assigned to the astigmatism of the thermal lens in N_g-cut MDT crystals [16]. The measured beam quality factors M^2_{xy} slightly increased with the pump power from ~1.1 near the laser threshold up to ~2 – 2.5 at full power.

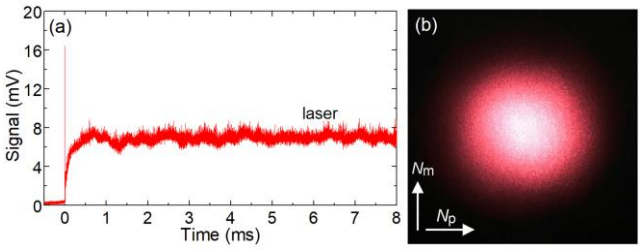

Fig. 7. $KEu(WO_4)_2$ laser (true CW operation): (a) typical oscilloscope trace of laser emisison; (b) photograph of the laser mode on a screen in the far-field (plano-plano cavity, T_{OC} = 0.3%).

In our experiments, the coatings of the cavity mirrors supported potential laser oscillations at the $^5D_0 \rightarrow {}^7F_2$ transition. However, despite higher SE cross-sections, lasing at this transition was not observed. We suggest two main reasons for that: (i) reabsorption related to transitions from the thermally populated state $^7F_2$ leading to quasi-three-level laser scheme and increased threshold and (ii) possible excited-state absorption from the metastable $^5D_0$ state (e.g., spin-allowed transition to the higher-lying $^5F_4$ excited-state which is estimated to occur at ~612 nm).

To conclude, we report on the first watt-level, highly efficient and low-threshold room-temperature Europium laser operating at the $^5D_0 \rightarrow {}^7F_4$ transition. It delivers 1.11 W at ~703 nm (falling in the deep-red spectral range) with a slope efficiency of 43.2% and a linear polarization. The laser threshold as low as 64 mW is also achieved utilizing the advantage of the quasi-four-level laser scheme. These output characteristics represent record values for any Eu lasers reported so far. This advance is based on the use of a stoichiometric $KEu(WO_4)_2$ crystal ensuring high absorption in the green and very weak luminescence quenching. Further power scaling in true CW regime seems feasible by appropriate thermal management of the crystal (e.g., active cooling). Further work should focus on revealing the possibility of RT laser operation at other Eu^{3+} transitions in the red (~0.62 μm, $^5D_0 \rightarrow {}^7F_2$) and deep red (~0.75 μm and ~0.81 μm, $^5D_0 \rightarrow {}^7F_{5,6}$). In the former case, ESA measurements are required.

Disclosures. The authors declare no conflicts of interest.

References

1. C. Kränkel, D. T. Marzahl, F. Moglia, G. Huber, and P. W. Metz, Laser Photon. Rev. **10**, 548 (2016).
2. R. P. Rao, Sol. State Commun. **99**, 439 (1996).
3. Z. Ju, R. Wei, X. Gao, W. Liu, and C. Pang, Opt. Mater. **33**, 909 (2011).
4. J. Zhong, D. Chen, H. Xu, W. Zhao, J. Sun, and Z. Ji, J. Alloys Compd. **695**, 311 (2017).
5. G. Jia, P. A. Tanner, C. K. Duan, and J. Dexpert-Ghys, J. Phys. Chem. C **114**, 2769 (2010).
6. N. C. Chang, J. Appl. Phys. **34**, 3500 (1963).
7. J. H. Park, and A. J. Steckl, Appl. Phys. Lett. **85**, 4588 (2004).
8. J. H. Park, and A. J. Steckl, J. Appl. Phys. **98**, 056108 (2005).
9. K. Nakamura, Y. Hasegawa, H. Kawai, N. Yasuda, N. Kanehisa, Y. Kai, T. Nagamura, S. Yanagida, and Y. Wada, J. Phys. Chem. A **111**, 3029 (2007).
10. S. N. Bagaev, V. I. Dashkevich, V. A. Orlovich, S. M. Vatnik, A. A. Pavlyuk, and A. M. Yurkin, Quantum Electron. **41**, 189 (2011).
11. V.I. Dashkevich, S.N. Bagayev, V.A. Orlovich, A.A. Bui, P.A. Loiko, K.V. Yumashev, N.V. Kuleshov, S.M. Vatnik, and A.A. Pavlyuk, Laser Phys. Lett. **12**, 015006 (2015).
12. V.I. Dashkevich, S.N. Bagayev, V.A. Orlovich, A.A. Bui, P.A. Loiko, K.V. Yumashev, A.S. Yasukevich, N.V. Kuleshov, S.M. Vatnik, and A.A. Pavlyuk, Laser Phys. Lett. **12**, 085001 (2015).
13. M. Demesh, A. Yasukevich, V. Kisel, E. Dunina, A. Kornienko, V. Dashkevich, V. Orlovich, E. Castellano-Hernández, C. Kränkel, and N. Kuleshov, Opt. Lett. **43**, 2364 (2018).
14. P. A. Loiko, V. I. Dashkevich, S. N. Bagaev, V. A. Orlovich, A. S. Yasukevich, K. V. Yumashev, N. V. Kuleshov, E. B. Dunina, A. A. Kornienko, S. M. Vatnik, and A. A. Pavlyuk, J. Lumin. **153**, 221 (2014).
15. V. Petrov, M. C. Pujol, X. Mateos, O. Silvestre, S. Rivier, M. Aguiló, R. M. Solé, J. Liu, U. Griebner, and F. Díaz, Laser & Photon. Rev. **1**, 179 (2007).
16. J. M. Serres, X. Mateos, P. Loiko, K. Yumashev, N. Kuleshov, V. Petrov, U. Griebner, M. Aguiló, and F. Díaz, Opt. Lett. **39**(14), 4247 (2014).
17. P. Pues, S. Schwung, D. Rytz, L. Schubert, S. Klenner, F. Stegemann, R. Poettgen, and T. Juestel, J. Lumin. **215**, 116653 (2019).

Full references

1. C. Kränkel, D. T. Marzahl, F. Moglia, G. Huber, and P. W. Metz, "Out of the blue: semiconductor laser pumped visible rare-earth doped lasers," Laser Photon. Rev. **10**(4), 548-568 (2016).
2. R. P. Rao, "Growth and characterization of Y_2O_3:Eu^{3+} phosphor films by sol-gel process," Sol. State Commun. **99**(6), 439-443 (1996).
3. Z. Ju, R. Wei, X. Gao, W. Liu, and C. Pang, "Red phosphor $SrWO_4$:Eu^{3+} for potential application in white LED," Opt. Mater. **33**(6), 909-913 (2011).
4. J. Zhong, D. Chen, H. Xu, W. Zhao, J. Sun, and Z. Ji, "Red-emitting $CaLa_4(SiO_4)_3O$:Eu^{3+} phosphor with superior thermal stability and high quantum efficiency for warm w-LEDs," J. Alloys Compd. **695**, 311-318 (2017).
5. G. Jia, P. A. Tanner, C. K. Duan, and J. Dexpert-Ghys, "Eu^{3+} spectroscopy: a structural probe for yttrium orthoborate phosphors," J. Phys. Chem. C **114**(6), 2769-2775 (2010).
6. N. C. Chang, "Fluorescence and stimulated emission from trivalent europium in yttrium oxide," J. Appl. Phys. **34**(12), 3500-3504 (1963).
7. J. H. Park, and A. J. Steckl, "Laser action in Eu-doped GaN thin-film cavity at room temperature," Appl. Phys. Lett. **85**(20), 4588-4590 (2004).
8. J. H. Park, and A. J. Steckl, "Demonstration of a visible laser on silicon using Eu-doped GaN thin films," J. Appl. Phys. **98**(5), 056108-1-3 (2005).
9. K. Nakamura, Y. Hasegawa, H. Kawai, N. Yasuda, N. Kanehisa, Y. Kai, T. Nagamura, S. Yanagida, and Y. Wada, "Enhanced lasing properties of dissymmetric Eu (III) complex with bidentate phosphine ligands," J. Phys. Chem. A **111**(16), 3029-3037 (2007).
10. S. N. Bagaev, V. I. Dashkevich, V. A. Orlovich, S. M. Vatnik, A. A. Pavlyuk, and A. M. Yurkin "25% Eu:$KGd(WO_4)_2$ laser crystal: spectroscopy and lasing on the $^5D_0 \rightarrow {}^7F_4$ transition," Quantum Electron. **41**(3), 189-192 (2011).
11. V.I. Dashkevich, S.N. Bagayev, V.A. Orlovich, A.A. Bui, P.A. Loiko, K.V. Yumashev, N.V. Kuleshov, S.M. Vatnik, and A.A. Pavlyuk, "Quasi-CW and CW laser operation of Eu:$KGd(WO_4)_2$ crystal on $^5D_0 \rightarrow {}^7F_4$ transition," Laser Phys. Lett. **12**(1), 015006-1-6 (2015).
12. V.I. Dashkevich, S.N. Bagayev, V.A. Orlovich, A.A. Bui, P.A. Loiko, K.V. Yumashev, A.S. Yasukevich, N.V. Kuleshov, S.M. Vatnik, and A.A. Pavlyuk, "Red Eu,Yb:$KY(WO_4)_2$ laser at ~702 nm," Laser Phys. Lett. **12**(8), 085001-1-5 (2015).
13. M. Demesh, A. Yasukevich, V. Kisel, E. Dunina, A. Kornienko, V. Dashkevich, V. Orlovich, E. Castellano-Hernández, C. Kränkel, and N. Kuleshov, "Spectroscopic properties and continuous-wave deep-red laser operation of Eu^{3+}-doped $LiYF_4$," Opt. Lett. **43**(10), 2364-2367 (2018).
14. P. A. Loiko, V. I. Dashkevich, S. N. Bagaev, V. A. Orlovich, A. S. Yasukevich, K. V. Yumashev, N. V. Kuleshov, E. B. Dunina, A. A. Kornienko, S. M. Vatnik, and A. A. Pavlyuk, "Spectroscopic and photoluminescence characterization of Eu^{3+}-doped monoclinic $KY(WO_4)_2$ crystal," J. Lumin. **153**, 221-226 (2014).
15. V. Petrov, M. C. Pujol, X. Mateos, O. Silvestre, S. Rivier, M. Aguiló, R. M. Solé, J. Liu, U. Griebner, and F. Díaz, "Growth and properties of $KLu(WO_4)_2$, and novel ytterbium and thulium lasers based on this monoclinic crystalline host," Laser & Photon. Rev. **1**(2), 179–212 (2007).
16. J. M. Serres, X. Mateos, P. Loiko, K. Yumashev, N. Kuleshov, V. Petrov, U. Griebner, M. Aguiló, and F. Díaz, "Diode-pumped microchip Tm:$KLu(WO_4)_2$ laser with more than 3 W of output power," Opt. Lett. **39**(14), 4247–4250 (2014).
17. P. Pues, S. Schwung, D. Rytz, L. Schubert, S. Klenner, F. Stegemann, R. Poettgen, and T. Juestel, "Temperature and time dependent photoluminescence of single crystalline $KEu(WO_4)_2$," J. Lumin. **215**, 116653-1-9 (2019).